



Detection band expansion by independently tunable double resonances in a long-wavelength dual-color QWIP

XU DAI,^{1,2} ZESHI CHU,^{1,2} JIE DENG,^{1,2} FANGZHE LI,¹ JING ZHOU,^{1,2,*}  DAYUAN XIONG,³ XIAOHAO ZHOU,^{1,2} XIAOSHUANG CHEN,^{1,2,4} NING LI,^{1,2} ZHIFENG LI,^{1,2}  WEI LU,^{1,2} AND XUECHU SHEN^{1,2}

¹State Key Laboratory of Infrared Physics, Shanghai Institute of Technical Physics, Chinese Academy of Sciences, 500 Yu Tian Road, Shanghai, 200083, China

²University of Chinese Academy of Sciences, 19 Yuquan Road, Beijing, 100049, China

³Key Laboratory of Polarized Materials and Devices, School of Physics and Electronic Science, East China Normal University, Shanghai 200241, China

⁴xschen@mail.sitp.ac.cn

*jzhou@mail.sitp.ac.cn

Abstract: Multi-resonance light coupling management is a promising way to expand the operating spectral ranges of optoelectronic devices. The classical strategies are either lack of independent tunability for each resonance or involved with complex fabrication. Here, we propose a new scheme for expanding the operating spectral range of an optoelectronic device through a dual-color active material integrated with a simple resonant waveguide structure. The TM waveguide mode and the SPP mode of the resonant waveguide structure are regulated to match the two active regions of the dual-color material both spectrally and spatially. Applying this scheme to a long-wavelength infrared quantum well photodetector, the absorption efficiencies at the two peak detection wavelengths of the dual-color quantum wells are both enhanced by more than 10 times compared with the case of a standard 45° edge facet coupled device with the same detection material. The simple light coupling structure is easy to accomplish and compatible with focal plane arrays. For thermal radiation detection, the absorption efficiency of the 300 K blackbody radiation by our dual-color detector is 83.8% higher than that by a single-color detector with the optimized structural parameters. Moreover, either polarization sensitive or polarization insensitive detection could be achieved in this dual-color infrared quantum well photodetector by using anisotropic or isotropic gratings.

© 2022 Optica Publishing Group under the terms of the [Optica Open Access Publishing Agreement](#)

1. Introduction

Light coupling management is one of the most important concerns of optoelectronic devices [1–8]. Especially for those based on low-dimensional active materials, integrated photonic structures are employed to generate locally intensified light fields at the active materials by resonances [5–9]. However, a single resonance usually corresponds to a limited operating spectral range. A lot of multi-resonance light couplers or absorbers have been proposed to enlarge operating spectral ranges [10–16], but achieving such a photonic structure still remains challenging, both in terms of design and fabrication. There are two classical strategies. One is to utilize the multiple orders of resonances of a photonic structure [16], but it is difficult to independently control the resonant wavelengths and field distributions of those resonances. The other is to combine multiple photonic structures together either horizontally or vertically [10–15], but it inevitably increases fabrication complexity and device sizes. Here, we report a new scheme of enlarging

the operating spectral range of an optoelectronic device through a dual-color active material enhanced by independently tunable double resonances of a simple resonant waveguide structure.

The optoelectronic device addressed detailedly in this study is a quantum well infrared photodetector (QWIP) working in the long-wavelength infrared (LWIR) range. Long-wavelength infrared detection is important for surveillance, industrial process control, medical imaging, and astronomy [17–19]. QWIPs have become a leading candidate for sensitive and cost-effective LWIR staring arrays [20,21] due to the mature processing techniques for III-V semiconductors, high uniformity of the epitaxial materials, tailorable detection wavelengths, radiation hardness [22,23]. However, the inherent narrow-band photoresponse is a shortcoming of QWIPs, especially for detecting thermal radiation, which is broadband. Thus, a detection band expansion of QWIPs becomes an appealing research topic [24–26]. Multicolor quantum well stacks with different photoresponse spectra provide a way for QWIPs to cover a wider spectral range [27,28]. How to efficiently couple the incident light of a specific wavelength to the corresponding quantum wells in the multicolor stacks remains a bottleneck problem [29,30]. Grating diffraction is commonly used in QWIPs, especially in QWIP focal plane arrays (FPAs) [17]. It is known that GaAs/AlGaAs QWIPs are only responsive to the light field with an electric component perpendicular to the GaAs/AlGaAs multiple layers [17–19]. Grating couplers usually deflect the incident light for an electric field component perpendicular to the QWs so that the light could be effectively absorbed by the QWs. Meanwhile, since the optical path of the deflected light is enlarged, the absorption efficiency of the QWs is enhanced. For multicolor QW stacks, higher-order diffractions of a grating coupler are exploited for shorter-wavelength QWs [16]. However, there are several shortcomings of this method: 1) The diffraction efficiency quickly decreases with diffraction order, so the QWs with shorter detection wavelengths cannot be effectively enhanced. 2) The wavelengths of different diffraction orders cannot be independently tuned to match the QWs of different colors. 3) In absence of resonances, the local field at the QWs is not intensified. In this work, we propose to use a waveguide mode and a surface plasmon polariton (SPP) mode supported by a simple resonant waveguide structure to enhance the absorption efficiency of an LWIR dual-color QWIP. In principle, the two peak detection wavelengths of the dual-color quantum wells can be arbitrarily set in the long wavelength infrared range. The light coupling structure is easy to fabricate and it is compatible with focal plane arrays. The semiconductor layer contains two QW stacks of different detection wavelengths (labeled as blue and red). Then the waveguide mode and the SPP mode can be independently manipulated to match the dual-color QW stacks both spectrally and spatially. As a result, the absorption efficiencies of the dual-color QW stacks are both enhanced by more than 10 times compared to the case of a 45° edge facet coupled QWIP (45°-QWIP) with the same detection material. Then, the detection band is effectively expanded. Concerning thermal radiation detection, the absorption efficiency of the 300 K blackbody radiation by our dual-color QWIP is 83.8% higher than that by a single-color QWIP with the optimized structural parameters. Moreover, either polarization sensitive or polarization insensitive detection could be achieved in the dual-color QWIPs by using anisotropic or isotropic gratings.

2. Results and discussions

As shown in Fig. 1(a), the dual-color QWIP consists of an etching stop layer (200 nm AlGaAs), a bottom contact layer (600 nm GaAs), 14 stacks of GaAs (5 nm)/Al_{0.24}Ga_{0.76}As (50 nm) (blue QWs), 14 stacks of GaAs (6 nm)/Al_{0.18}Ga_{0.82}As (50 nm) (red QWs), and a top contact layer (580 nm GaAs). A light coupling grating is created by etching the top contact layer and coating the surface with metal. The grating period (Λ) is 3.2 μm , the grating width (g) is 1.5 μm , and the depth (h) is 380 nm. Then, the semiconductor layers together with the grating form a resonant waveguide. The air and the metal serve as the cladding, and the semiconductor part serves as the core. The thickness of the waveguide core (d) is defined as the thickness of all the semiconductor

layers minus h . Figure 1 (a) shows the flipped-chip structure of the dual-color QWIP that is ready for connection with readout circuits. The blue and red QW stacks have two different detection bands in the LWIR range. The multiple QWs could be regarded as an effective uniaxial medium with a diagonal dielectric constant tensor [17,33,34]. $\epsilon_{\text{QW}} = \text{diag}(\epsilon_x, \epsilon_y, \epsilon_z)$, where $\epsilon_z = \epsilon_{\text{GaAs}} + 0.5\omega\gamma/(\omega_0^2 - \omega^2 - i\omega\gamma)$. The x - y plane is parallel to the multilayers, and the z -axis is perpendicular to them. For the light field polarized parallel to the x - y plane, the effective medium of the QWs behaves like GaAs, which is a dielectric with a slowly varying real dielectric constant within the LWIR range. For the light field polarized along the z -axis, the intersubband transition is active so the effective medium behaves as a Lorentz oscillator. $\hbar\omega_0$ corresponds to the intersubband energy difference. γ is the damping frequency and is estimated to be $0.05\omega_0$ in our case [24,31,32]. Assuming the peak absorption efficiency wavelengths of the blue and the red QWs are $8.5\ \mu\text{m}$ and $10.5\ \mu\text{m}$, respectively, the real and imaginary parts of the wavelength dependent z -component dielectric constants (ϵ_z) are shown in Fig. 1(b). The refractive index of GaAs takes 3.27. The thickness of the GaAs top contact (excluding the grating) is $200\ \text{nm}$ and that of the bottom contact is $600\ \text{nm}$. The permittivity of gold follows the Drude model. Figure 1 (c) shows the absorption efficiency of the 45° edge facet coupled dual-color QWIP (45° -QWIP).

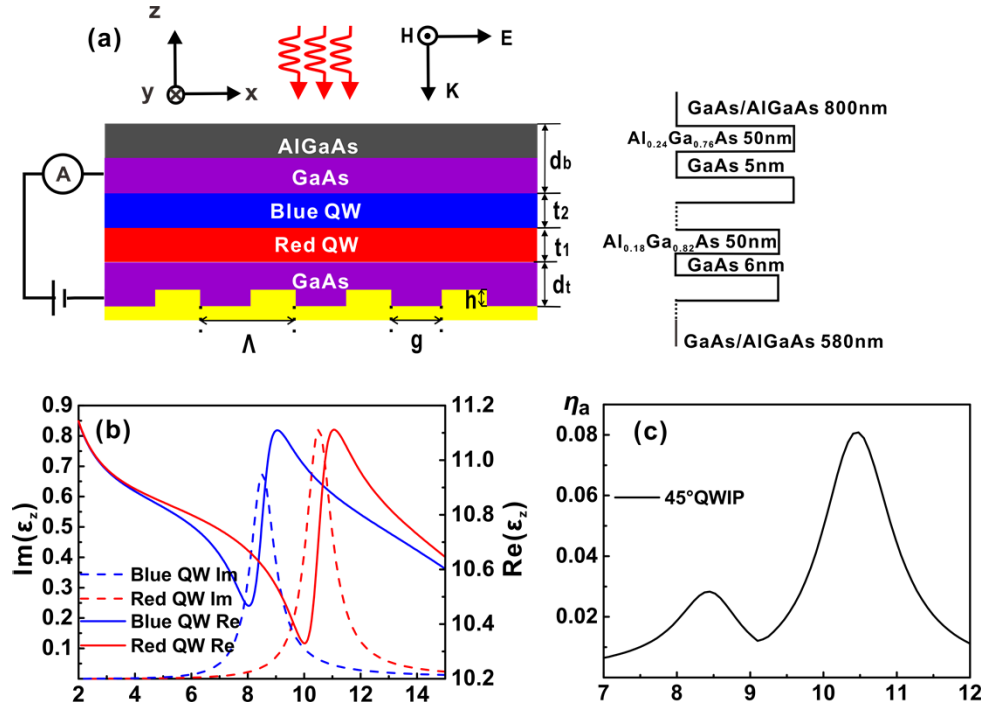


Fig. 1. (a) Schematic of the resonant waveguide integrated dual-color long-wavelength QWIP. $d_b = 0.8\ \mu\text{m}$, $t_2 = 0.8\ \mu\text{m}$, $t_1 = 0.8\ \mu\text{m}$, $d_t = 0.58\ \mu\text{m}$, $h = 0.38\ \mu\text{m}$, $\Lambda = 3.2\ \mu\text{m}$, $g = 1.5\ \mu\text{m}$. The right panel is the band diagram of the QWs and contacts. (b) Real and imaginary parts of ϵ_z . (c) Absorption efficiency (η_a) of the 45° -QWIP. The two absorption peaks correspond to the two peak detection wavelengths of the dual-color QWs.

The resonant waveguide with a metal-coated grating can hold waveguide modes and an SPP mode. It is known that the excitation of a TM waveguide mode or an SPP mode that spectrally matches the photosensitive spectral range of the QWs can prominently enhance the absorption efficiency of the QWs since the local field with a z -direction electric component in the QWs is resonantly intensified [19,24–26]. Here, in the dual-color QWIP, there are two stacks of QWs

with two different detection wavelengths. And we propose to utilize the 1st TM mode and the SPP mode to enhance the absorption efficiency in the blue and red QW stacks, respectively. The key issue is to ensure that these two light modes match the two stacks of QWs both spectrally and spatially. The excitation of either the 1st TM mode or the SPP mode requires that the lateral wave vector of the incident light (k_x) equals the propagation constant (β_{TM1} or β_{SPP}). Concerning normal incidence, with the help of the grating, k_x equals $\pm 2m\pi/\Lambda$. Here, we only consider the first order diffraction of the grating ($m = 1$) since higher order diffractions typically correspond to lower efficiency. Thus, with a single grating structure, the propagation constants of the 1st TM mode and the SPP mode that can be excited by a normally incident light fulfills the equation $\beta_{\text{TM1}} = \beta_{\text{SPP}} = \pm 2\pi/\Lambda$. Then, the resonant wavelengths of these two modes are determined by the following equations:

$$\kappa d - \phi_1 - \phi_2 = m\pi, \quad (1)$$

$$\kappa = (\varepsilon_{\text{III-V}} k_0^2 - \beta^2)^{1/2}, \quad (2)$$

$$\phi_1 = \arctan(\varepsilon_{\text{III-V}} \alpha_{\text{Au}} / \varepsilon_{\text{Au}} \kappa), \quad (3)$$

$$\phi_2 = \arctan(\varepsilon_{\text{III-V}} \alpha_{\text{air}} / \varepsilon_{\text{air}} \kappa). \quad (4)$$

κ denotes the z component of the wave vector in the semiconductor layers, $(-\phi_1)$ or $(-\phi_2)$ half the gained reflection phase at the semiconductor-air interface or at the semiconductor-metal interface, m an integer corresponding to the order of the light mode, $\varepsilon_{\text{III-V}}$ the dielectric constant of the semiconductor layers ($\varepsilon_{\text{III-V}} \approx \varepsilon_{\text{GaAs}}$), ε_{Au} the dielectric constant of gold, ε_{air} the dielectric constant of air, k_0 the wave vector in free space, $\alpha_{\text{Au}} = (\beta^2 - k_0^2 \varepsilon_{\text{Au}})^{1/2}$, and $\alpha_{\text{air}} = (\beta^2 - k_0^2 \varepsilon_{\text{air}})^{1/2}$. Equation (1) is a transcendental equation of β . When $m = 0$, Eq. (1) describes the dispersion relation of the SPP mode [35,36], and $\beta = \beta_{\text{SPP}}$. When $m = 1$, Eq. (1) describes the dispersion relation of the 1st TM mode, and $\beta = \beta_{\text{TM1}}$. Either for the 1st TM mode or the SPP mode, an absorption peak is formed at the resonant wavelength (λ_{TM} or λ_{SPP}), as shown in Fig. 2 (a). With the varying period of the grating, the absorption peak moves in the spectrum, and the trajectory reflects the dispersion relation of this mode. The left contour in Fig. 2 (a) represents the period-wavelength-dependent absorption efficiency of the blue QW stack ($\eta_{a\text{-blue}}$) and the right contour represents the absorption efficiency of the red QW stack ($\eta_{a\text{-red}}$). It is revealed that either $\eta_{a\text{-blue}}$ or $\eta_{a\text{-red}}$ reaches a maximum when λ_{TM} or λ_{SPP} matches the intrinsic absorption peak wavelength of the blue or red QW stack (λ_{blue} or λ_{red}). Then, if λ_{TM} and λ_{SPP} could simultaneously match λ_{blue} and λ_{red} , respectively, at the same grating period, the dual-color QWIP should work in an excellent condition. Although the propagation constants of the two light modes are fixed by the same grating ($\beta_{\text{TM1}} = \beta_{\text{SPP}} = \pm 2\pi/\Lambda$), the dispersion relations can be tuned separately to make $\lambda_{\text{TM}} = \lambda_{\text{blue}}$ and $\lambda_{\text{SPP}} = \lambda_{\text{red}}$. According to Eq. (1), the waveguide thickness d is a critical parameter that controls the dispersion relations of the two light modes. As shown in Fig. 2 (b), the dispersion relation of the SPP mode is much less influenced by d than that of the 1st TM mode. In addition, the reflection phase at the semiconductor-metal interface can be tuned by adjusting the grating geometry such as the period and the duty cycle. So we could make the SPP resonances at different d values almost follow the same dispersion, as shown by the squares in Fig. 2 (b). Thus, if the grating period is fixed, adjusting d could sensitively shift the resonance of the 1st TM mode but hardly affects the resonance of the SPP mode. In this case, it is feasible and straightforward to design a structure by which λ_{TM} and λ_{SPP} match λ_{blue} and λ_{red} , respectively. As shown in Fig. 2 (a), when $\Lambda = 3.2 \mu\text{m}$ and $d = 2.6 \mu\text{m}$, λ_{TM} matches λ_{blue} at $8.5 \mu\text{m}$ and λ_{SPP} matches λ_{red} at $10.5 \mu\text{m}$. Thus, $\eta_{a\text{-blue}}$ is enhanced to 81.5% and $\eta_{a\text{-red}}$ is enhanced to 77.7%. As a comparison, for the 45°-QWIP, $\eta_{a\text{-blue}}$ is only 2.8% and $\eta_{a\text{-red}}$ is 8.1%. In principle, even though λ_{blue} and λ_{red} are arbitrarily distributed in the wavelength range, a proper set of Λ and d can always be found to match λ_{TM} and λ_{SPP} with λ_{blue} and λ_{red} , respectively. As shown in Fig. 2 (c), when λ_{blue} and λ_{red} become closer, the optimized grating period ($\Lambda = 3.2 \mu\text{m}$) and waveguide thickness ($d = 3.8 \mu\text{m}$) can still result in high absorption

efficiencies ($\eta_{a\text{-blue}} = 80.3\%$ and $\eta_{a\text{-red}} = 73.7\%$). Similarly, when λ_{blue} and λ_{red} become farther apart (Fig. 2 (d)), the optimized grating period ($\Lambda = 3.8 \mu\text{m}$) and waveguide thickness ($d = 2.2 \mu\text{m}$) also result in high absorption efficiencies ($\eta_{a\text{-blue}} = 74.4\%$ and $\eta_{a\text{-red}} = 77.2\%$). The optimized total absorption efficiency (η_a) spectra of the three dual-color QWIPs are presented in Fig. 2 (e).

The absorption efficiency enhancement of the dual-color QWIP is not only attributed to the matching of λ_{TM} (λ_{SPP}) and λ_{blue} (λ_{red}), but also to the fact that the light fields of the 1st TM mode and the SPP mode are mainly distributed in the blue QW stack and the red QW stack, respectively. Since the semiconductor layers of the dual-color QWIP are grown by epitaxy, the stacking order of these layers can be manipulated. In our device, the blue QW stack is placed in the middle of the waveguide layer, corresponding to the local field of the 1st TM mode. The red QW stack is placed closer to the Au/GaAs interface since the light field of the SPP mode is mainly distributed in the vicinity of the metal surface. During the material growth process, the blue QW stack should be grown before the red one, which can be easily realized by a typical molecular beam epitaxy system. As shown in Fig. 3 (a), for the incident light with a wavelength of $8.5 \mu\text{m}$, the 1st TM mode is excited in the resonant waveguide integrated dual-color QWIP. The local field of the 1st TM mode is mainly concentrated at the blue QW stack. Since the GaAs/AlGaAs QWs only absorb the light component polarized along the z -direction, the absorption efficiency of the QWs is proportional to $|E_z|^2$, and thus $|E_z|^2$ becomes an indicator of the light coupling condition. To quantitatively describe the light coupling efficiency in the QWs, the z -dependent absorbable field enhancement, defined as

$$\frac{\langle |E_z|^2 \rangle}{\langle |E_0|^2 \rangle} = \frac{\iint |E_z|^2 dx dy}{\iint |E_0|^2 dx dy} \quad (5)$$

is calculated. The integral region of the above formula is the whole x - y plane at a specific z position. As shown in Fig. 3 (b), the light field of the 1st TM mode is mainly distributed in the blue QW stack. The field enhancement factor $\langle |E_z|^2 \rangle / \langle |E_0|^2 \rangle$ is averagely higher than 10 within this active region. For the incident light with a wavelength of $10.5 \mu\text{m}$, the SPP mode is excited at the interface between the coated metal and the GaAs contact layer. As shown in Fig. 3 (c) and (d), since the red QW stack is very close to the Au/GaAs interface, the light field within the red QW stack is prominently enhanced. The highest $\langle |E_z|^2 \rangle / \langle |E_0|^2 \rangle$ value in this active region reaches 16, indicating that the absorption efficiency of the red QW stack can be remarkably increased by the SPP mode. Therefore, the 1st TM mode and the SPP mode not only spectrally but also spatially match the blue and red QW stacks, respectively, and thus the absorption efficiency of the dual-color QWIP is prominently enhanced in both the two detection ranges.

The remarkably expanded detection range in the LWIR regime is favored for room temperature thermal radiation detection. The thermal radiation arriving at the detector at normal incidence is expressed as:

$$P = \int \varepsilon B(\lambda, T) d\lambda, \quad (6)$$

where ε denotes the emissivity of this object, and $B(\lambda, T)$ denotes the blackbody radiation energy density (Fig. 4 (a) black line). When the temperature is 300 K, the peak wavelength of blackbody radiation is about $9.7 \mu\text{m}$, and the FWHM is $11.59 \mu\text{m}$. Then, the absorption efficiency of the blackbody radiation in the QWs writes

$$A_{\text{QW}} = \frac{\int \eta_a(\lambda) \varepsilon B(\lambda, T) d\lambda}{\int \varepsilon B(\lambda, T) d\lambda}. \quad (7)$$

To get a high responsivity, a broad and high $\eta_a(\lambda)$ is pursued. Concerning a typical single color LWIR QWIP with an absorption peak at the wavelength of $9.7 \mu\text{m}$, which is consistent with the peak wavelength of blackbody radiation at 300 K, the detection range is about $0.72 \mu\text{m}$, only

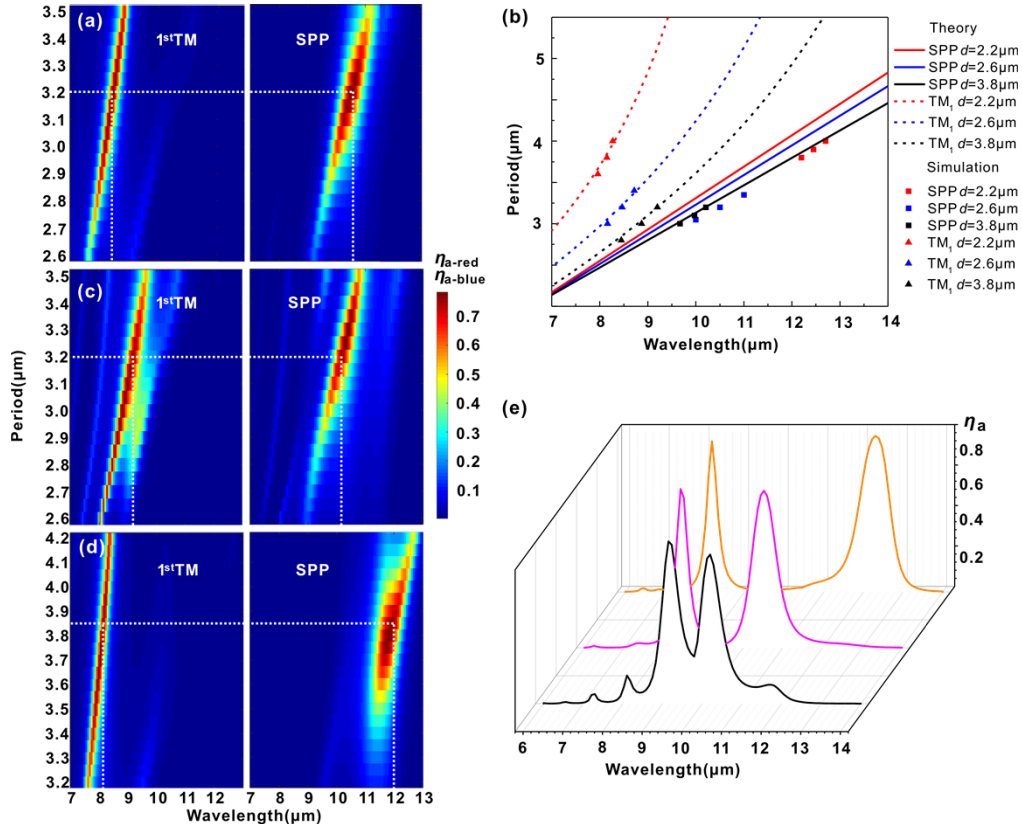


Fig. 2. (a), (c) and (d) Grating period dependent spectra of $\eta_{a\text{-blue}}$ (left) and $\eta_{a\text{-red}}$ (right) of three grating coupled dual-color QWIPs. (a): $d = 2.6 \mu\text{m}$, $\Lambda = 3.2 \mu\text{m}$, $g = 1.5 \mu\text{m}$, $d_t = 0.58 \mu\text{m}$, $h = 0.38 \mu\text{m}$, $t_2 = 0.8 \mu\text{m}$, $t_1 = 0.8 \mu\text{m}$, $d_b = 0.8 \mu\text{m}$, $\lambda_{\text{blue}} = 8.5 \mu\text{m}$, and $\lambda_{\text{red}} = 10.5 \mu\text{m}$. (c): $d = 3.8 \mu\text{m}$, $\Lambda = 3.2 \mu\text{m}$, $g = 1.9 \mu\text{m}$, $d_t = 0.73 \mu\text{m}$, $h = 0.53 \mu\text{m}$, $t_2 = 1.3 \mu\text{m}$, $t_1 = 1.5 \mu\text{m}$, $d_b = 0.8 \mu\text{m}$, $\lambda_{\text{blue}} = 9.2 \mu\text{m}$, and $\lambda_{\text{red}} = 10.2 \mu\text{m}$. (d): $d = 2.2 \mu\text{m}$, $\Lambda = 3.8 \mu\text{m}$, $g = 2.25 \mu\text{m}$, $d_t = 0.58 \mu\text{m}$, $h = 0.38 \mu\text{m}$, $t_2 = 0.8 \mu\text{m}$, $t_1 = 0.95 \mu\text{m}$, and $d_b = 0.25 \mu\text{m}$, $\lambda_{\text{blue}} = 8.2 \mu\text{m}$, and $\lambda_{\text{red}} = 12.2 \mu\text{m}$. (b) Dispersion curves of the SPP mode and the 1st TM mode of the grating coupled dual-color QWIPs with different d values. The lines are predicted by Eq. (1). The scatters are based on the simulation results in (a), (c), and (d). (e) Spectra of the total absorption efficiency (η_a) of the three QWIPs in (a), (c) and (d) with the optimized structure parameters, by which the peak wavelengths of the three η_a spectra match the three sets of λ_{blue} and λ_{red} , respectively.

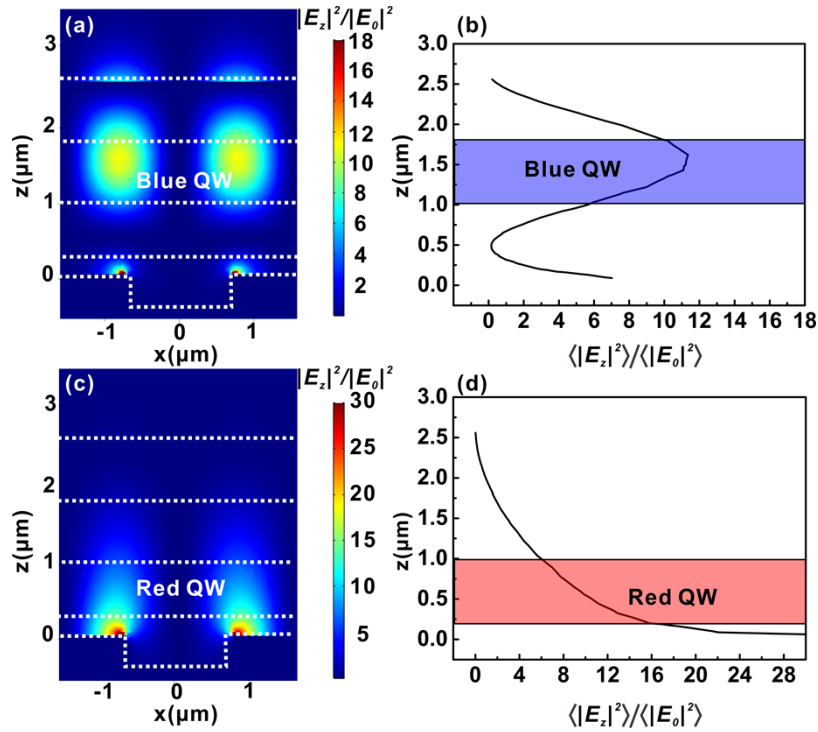


Fig. 3. (a) and (c) Simulated $|E_z|^2/|E_0|^2$ distributions in the x - z plane of the dual-color QWIP device ($\Lambda = 3.2 \mu\text{m}$, $g = 1.5 \mu\text{m}$, $d_t = 0.58 \mu\text{m}$, $h = 0.38 \mu\text{m}$, $t_2 = 0.8 \mu\text{m}$, $t_1 = 0.8 \mu\text{m}$, and $d_b = 0.8 \mu\text{m}$) at the wavelengths of $8.5 \mu\text{m}$ and $10.5 \mu\text{m}$, respectively. (b) and (d) Field enhancement factor as a function of the distance (z) from the grating at $8.5 \mu\text{m}$ and $10.5 \mu\text{m}$, respectively.

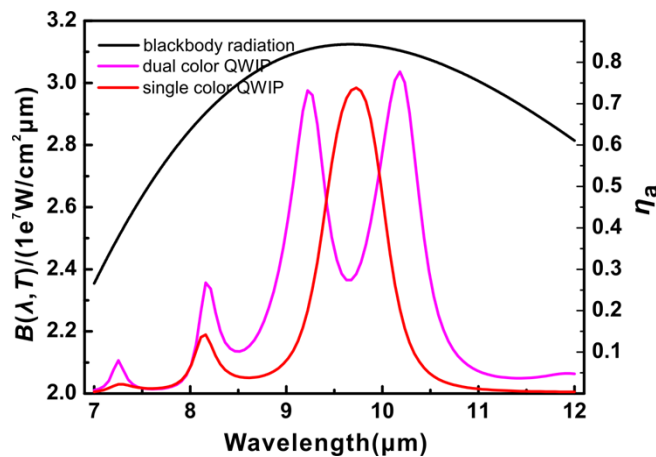


Fig. 4. Blackbody radiation energy density at 300 K (black line) and absorption efficiency of our dual-color detector (pink line) and the single-color detector (red line).

6.2% of the FWHM of the blackbody radiation spectrum. Thus, 93.8% of the blackbody thermal radiation signal is wasted even though it reaches the detector. This single color QWIP consists of 28 periods of quantum wells, whose total thickness is 1.6 μm . The QWIP is integrated with a typical grating coupler ($\Lambda = 3.0 \mu\text{m}$, $g = 1.8 \mu\text{m}$, $d_t = 0.58 \mu\text{m}$, $h = 0.38 \mu\text{m}$, $t_2 = 0.8 \mu\text{m}$, $t_1 = 0.8 \mu\text{m}$, and $d_b = 0.8 \mu\text{m}$). With these optimized structure parameters, the peak absorption efficiency at 9.7 μm reaches 73.7%.

The double-resonance-enhanced dual-color QWIP provides a new opportunity. As shown in Fig. 4, the double-peak η_a spectrum leads to a total absorption efficiency much higher than that of the single color QWIP. As listed in Table 1, the absorption efficiency of the 300 K thermal radiation in the dual-color QWIP is 83.8% higher than that of the single color QWIP. As the temperature of the thermal radiation increases, the peak wavelength of the radiation is blue-shifted, so the absorption efficiency enhancement $(A_{\text{QW-dual}} - A_{\text{QW-single}})/A_{\text{QW-single}}$ provided by the dual-color QWIP slightly decreases. But it is still as high as 83.4% at the thermal radiation temperature of 500 K. $A_{\text{QW-dual}}$ denotes the blackbody radiation absorption efficiency of the dual-color detector ($\lambda_{\text{blue}} = 9.2 \mu\text{m}$, $\lambda_{\text{red}} = 10.2 \mu\text{m}$). $A_{\text{QW-single}}$ denotes the blackbody radiation absorption efficiency of the single color detector with a peak absorption efficiency of 9.7 μm .

Table 1. Absorption efficiency of thermal radiation in the dual-color QWIP and the single-color QWIP at different temperatures

Temperature	$A_{\text{QW-dual}}$	$A_{\text{QW-single}}$	$(A_{\text{QW-dual}} - A_{\text{QW-single}})/A_{\text{QW-single}}$
300K	0.2568	0.1397	0.8382
400K	0.2460	0.1342	0.8331
500K	0.2372	0.1293	0.8345

The dual-color infrared detector based on the double resonances of the resonant waveguide structure could be either polarization sensitive or insensitive by using anisotropic or isotropic coupling gratings. As shown in Fig. 5 (a), the polarization extinction ratio $\eta_{\alpha-TM}/\eta_{\alpha-TE}$ of the dual-color QWIP with a 1D grating (Fig. 5 (c)) is larger than 1900 at both the wavelengths of 8.5 μm and 10.5 μm . The high polarization discrimination is attributed to the combined effect of the intrinsic polarization selectivity of the QWs and the polarization dependent coupling of the 1D grating [6,9,32]. Since GaAs/AlGaAs QWIPs are only responsive to the light field with an electric component perpendicular to the GaAs/AlGaAs multiple layers [17–19], only the TM modes and the SPP mode can be absorbed by the QWs, while the TE modes cannot. Moreover, the 1D grating serves as a polarization selective coupler. The TM modes and the SPP mode can only be excited by the incident light with an electric component along the x -direction, while the y -polarized incident light can only excite TE modes that cannot be absorbed by the QWs. Once the grating is changed into a 2D form (Fig. 5 (d)), the x -polarized and the y -polarized incident light are the same for the detector. As shown in Fig. 5 (b), the incident light from the two polarization directions, and the absorption efficiency spectrum of QWIP is exactly the same. Both of them can excite the TM modes and the SPP mode.

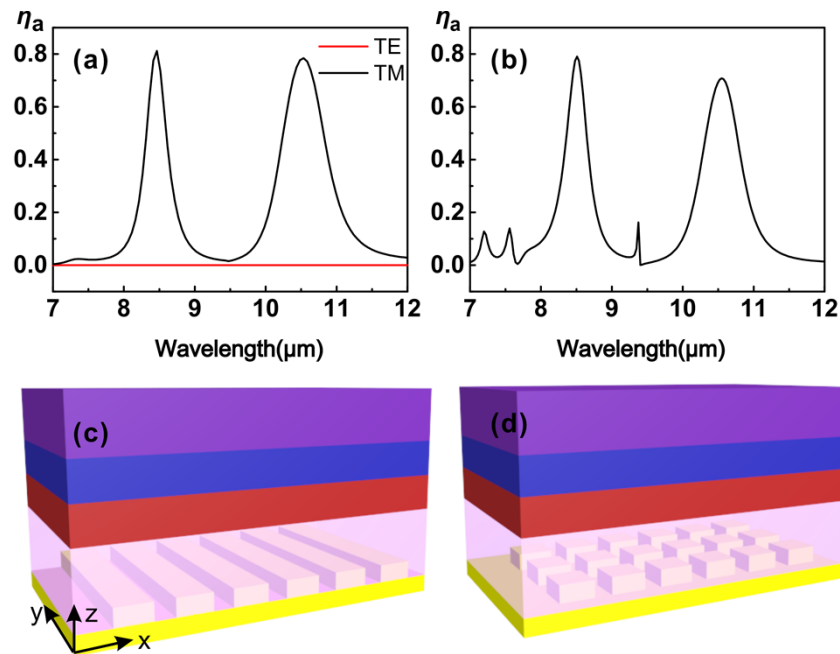


Fig. 5. (a)-(b) Absorption efficiency spectra of the double-resonance-enhanced dual-color QWIP with a 1D grating (a) and a 2D grating (b) under illumination of TE and TM waves. (c)-(d) Sketches of the double-resonance-enhanced dual-color QWIP with a 1D grating (c) and a 2D grating (d).

3. Conclusion

In summary, we propose a new scheme of using independently tunable guided mode resonance and SPP resonance to enhance a dual-color LWIR QWIP for detection band expansion. The double resonances are supported by a simple resonant waveguide structure. In the frequency domain, the resonant waveguide mode and the SPP mode can be separately tuned to match the two detection wavelength ranges of the two QW stacks, respectively. In the spatial domain, the two light modes are mainly distributed in the corresponding QW stacks. In this way, the absorption efficiencies of the two QW stacks are both enhanced by more than 10 times and thus the detection band is effectively expanded. Besides, the device structure is easy to fabricate, and compatible with focal plane arrays. Concerning the detection of room temperature thermal radiation, the double-resonance-enhanced dual-color QWIP absorbs 83.8% more power than a grating coupled single-color QWIP with the optimized structural parameters. Further, the device could be highly polarization discriminative or polarization insensitive by switching between one- or two-dimensional grating structures.

Funding. National Key Research and Development Program of China (2018YFA0306200); National Natural Science Foundation of China (61874126, 61975223, 91850208, 61991442); Hundred Talents Program of the Chinese Academy of Sciences (No. 20181214); Key Deployment Projects of the Chinese Academy of Sciences (ZDRW-XH-2021-7-1); Program of Shanghai Academic Research Leader (22XD1424400); Shanghai Municipal Science and Technology Major Project (Grant No.2019SHZDZX01).

Acknowledgments. This work was supported by the [Shanghai Tech University Quantum Device Lab \(SQDL\)](#).

Disclosures. The authors declare no conflicts of interest.

Data availability. Data underlying the results presented in this paper are not publicly available at this time but may be obtained from the authors upon reasonable request.

References

1. R.-N. Wu, C.-C. Ni, S. Yang, Y. Kuo, W.-Y. Chang, Y.-C. Su, S.-Y. Kuo, and C. C. Yang, "Surface Plasmon Coupling of Ag Nanoparticles with InGaN/GaN Quantum Wells for Enhancing the Emission Efficiency of Light-Emitting Devices," *ACS Appl. Nano Mater.* **5**(6), 8288–8297 (2022).
2. T. Shi, Z.-L. Deng, G. Geng, X. Zeng, Y. Zeng, G. Hu, A. Overvig, J. Li, C.-W. Qiu, A. Alù, Y. S. Kivshar, and X. Li, "Planar chiral metasurfaces with maximal and tunable chiroptical response driven by bound states in the continuum," *Nat. Commun.* **13**(1), 4111 (2022).
3. Z. Ren, Z. Zhang, J. Wei, B. Dong, and C. Lee, "Wavelength-multiplexed hook nanoantennas for machine learning enabled mid-infrared spectroscopy," *Nat. Commun.* **13**(1), 3859 (2022).
4. H. Qian, S. Li, S.-W. Hsu, C.-F. Chen, F. Tian, A. R. Tao, and Z. Liu, "Highly-efficient electrically-driven localized surface plasmon source enabled by resonant inelastic electron tunneling," *Nat. Commun.* **12**(1), 3111 (2021).
5. I. Epstein, D. Alcaraz, Z. Huang, V.-V. Pusapati, J.-P. Hugonin, A. Kumar, X. M. Deputy, T. Khodkov, T. G. Rappoport, J.-Y. Hong, N. M. R. Peres, J. Kong, D. R. Smith, and F. H. L. Koppens, "Far-field excitation of single graphene plasmon cavities with ultracompressed mode volumes," *Science* **368**(6496), 1219–1223 (2020).
6. S. Guo, D. Zhang, J. Zhou, J. Deng, Y. Yu, J. Deng, Q. Cai, Z. Li, W. Lu, and X. Chen, "Enhanced infrared photoresponse induced by symmetry breaking in a hybrid structure of graphene and plasmonic nanocavities," *Carbon* **170**, 49–58 (2020).
7. S. N. Gupta, O. Bitton, T. Neuman, R. Esteban, L. Chuntonov, J. Aizpurua, and G. Haran, "Complex plasmon-exciton dynamics revealed through quantum dot light emission in a nanocavity," *Nat. Commun.* **12**(1), 1310 (2021).
8. Y. Li, N. An, Z. Lu, Y. Wang, B. Chang, T. Tan, X. Guo, X. Xu, J. He, H. Xia, Z. Wu, Y. Su, Y. Liu, Y. Rao, G. Soavi, and B. Yao, "Nonlinear co-generation of graphene plasmons for optoelectronic logic operations," *Nat. Commun.* **13**(1), 3138 (2022).
9. J. Deng, Y. Zheng, J. Zhou, Z. Li, S. Guo, X. Dai, Y. Yu, Z. Ji, Z. Chu, X. Chen, and W. Lu, "Absorption enhancement in all-semiconductor plasmonic cavity integrated THz quantum well infrared photodetectors," *Opt. Express* **28**(11), 16427–16438 (2020).
10. L. Zeng, X. Zhang, H. Ye, H. Dong, and H. Zhang, "Design of ultra-broadband absorption enhancement in plasmonic absorber by interaction resonance of multi-plasmon modes and Fabry-Perot mode," *Opt. Express* **29**(18), 29228–29241 (2021).
11. L. Yu, Y. Liang, H. Gao, K. Kuang, Q. Wang, and W. Peng, "Multi-resonant absorptions in asymmetric step-shaped plasmonic metamaterials for versatile sensing application scenarios," *Opt. Express* **30**(2), 2006–2017 (2022).
12. C. Zhang, S. Yin, C. Long, B. W. Dong, D. He, and Q. Cheng, "Hybrid metamaterial absorber for ultra-low and dual-broadband absorption," *Opt. Express* **29**(9), 14078–14086 (2021).
13. Z. Li, L. Fan, H. Zhao, Y. Yan, and J. Gao, "Optical properties and application potential of a hybrid cavity compound grating structure," *Opt. Express* **30**(5), 7737–7749 (2022).
14. Z. Qin, X. Shi, F. Yang, E. Hou, D. Meng, C. Sun, R. Dai, S. Zhang, H. Liu, H. Xu, and Z. Liang, "Multi-mode plasmonic resonance broadband LWIR metamaterial absorber based on lossy metal ring," *Opt. Express* **30**(1), 473–483 (2022).
15. H. Zhu, Y. Zhang, L. Ye, Y. Li, Y. Xu, and R. Xu, "Switchable and tunable terahertz metamaterial absorber with broadband and multi-band absorption," *Opt. Express* **28**(26), 38626–38637 (2020).
16. M. Z. Tidrow, K. K. Choi, A. J. DeAnni, W. H. Chang, and S. P. Svensson, "Grating coupled multicolor quantum well infrared photodetectors," *Appl. Phys. Lett.* **67**(13), 1800–1802 (1995).
17. H. Schneider and H. C. Liu, *Quantum Well Infrared Photodetectors: Physics and Applications*, Springer Series in Optical Sciences No. 126 (Springer, 2007).
18. A. Krier, eds., *Mid-Infrared Semiconductor Optoelectronics*, Springer Series in Optical Sciences No. 118 (Springer, 2006).
19. S. S. Li and Y.-K. Su, eds., *Intersubband Transitions in Quantum Wells: Physics and Devices* (Springer US, 1998).
20. A. Rogalski, "Material considerations for third generation infrared photon detectors," *Infrared Phys. Technol.* **50**(2-3), 240–252 (2007).
21. A. W. van Herwaarden, F. G. van Herwaarden, S. A. Molenaar, E. J. G. Goudena, M. Laros, P. M. Sarro, C. A. Schot, W. van der Vlist, L. Blarke, and J. P. Krebs, "Design and fabrication of infrared detector arrays for satellite attitude control," *Sens. Actuators, A* **83**(1-3), 101–108 (2000).
22. C. Downs and T. Vandervelde, "Progress in Infrared Photodetectors Since 2000," *Sensors* **13**(4), 5054–5098 (2013).
23. Z. Shi, L. Wang, H. Zhen, W. Wang, and H. Chen, "Molecular beam epitaxy growth of peak wavelength-controlled InGaAs/AlGaAs quantum wells for 4.3- μm mid-wavelength infrared detection," *Nanoscale Res. Lett.* **8**(1), 310 (2013).
24. W. Tang, J. Zhou, Y. Zheng, Y. Zhou, J. Hao, X. Chen, and W. Lu, "All-dielectric resonant waveguide based quantum well infrared photodetectors for hyperspectral detection," *Opt. Commun.* **427**, 196–201 (2018).
25. H. Wang, H. Zhen, S. Li, Y. Jing, G. Huang, Y. Mei, and W. Lu, "Self-rolling and light-trapping in flexible quantum well-embedded nanomembranes for wide-angle infrared photodetectors," *Sci. Adv.* **2**(8), e1600027 (2016).
26. Y. Zhou, Z. Li, X. Zhou, J. Zhou, Y. Zheng, L. Li, N. Li, P. Chen, X. Chen, and W. Lu, "Cut-off wavelength manipulation of pixel-level plasmonic microcavity for long wavelength infrared detection," *Appl. Phys. Lett.* **114**(6), 061104 (2019).

27. X. Bai, P. Bai, X. Li, S. Huang, X. Lian, W. Song, Z. Shi, W. Shen, and Y. Zhang, "Optical coupling enhancement of multi-color terahertz quantum well detector," *J. Appl. Phys.* **130**(20), 203102 (2021).
28. L. Yue, Y. Wang, Z. Cui, X. Zhang, Y. Zhu, X. Zhang, S. Chen, X. Wang, and K. Zhang, "Multi-band terahertz resonant absorption based on an all-dielectric grating metasurface for chlorpyrifos sensing," *Opt. Express* **29**(9), 13563–13575 (2021).
29. Alexander Soibel, Ed Luong, Jason M. Mumolo, John Liu, Sir B. Rafol, Sam A. Keo, William Johnson, Dan Willson, Cory J. Hill, David Z.-Y. Ting, and Sarath D. Gunapala "Multi-color QWIP FPAs for hyperspectral thermal emission instruments", Proc. SPIE 8631, Quantum Sensing and Nanophotonic Devices X, 86310R (4 February 2013).
30. M. Sundaram, S. C. Wang, M. F. Taylor, A. Reisinger, G. L. Milne, K. B. Rei, R. E. Rose, and R. R. Martin, "Two-color quantum well infrared photodetector focal plane arrays," *Infrared Phys.* **42**(3-5), 301–308 (2001).
31. T. Zhen, J. Zhou, Z. Li, and X. Chen, "Realization of Both High Absorption of Active Materials and Low Ohmic Loss in Plasmonic Cavities," *Adv. Opt. Mater.* **7**(11), 1801627 (2019).
32. Z. Chu, J. Zhou, X. Dai, F. Li, M. Lan, Z. Ji, W. Lu, and X. Chen, "Circular Polarization Discrimination Enhanced by Anisotropic Media," *Adv. Opt. Mater.* **8**(9), 1901800 (2020).
33. C. Zhang, H. Chang, F. Zhao, and X. Hu, "Design principle of Au grating couplers for quantum-well infrared photodetectors," *Opt. Lett.* **38**(20), 4037–4039 (2013).
34. Z. Chu, Y. Zhou, J. Zhou, P. Chen, Z. Li, W. Lu, and X. Chen, "Quantum well infrared detectors enhanced by faceted plasmonic cavities," *Infrared Phys. Technol.* **116**, 103746 (2021).
35. K. Okamoto, "Chapter 1 - Wave theory of optical waveguides," in *Fundamentals of Optical Waveguides (Second Edition)*, K. Okamoto, ed. (Academic Press, 2006), pp. 1–12.
36. A. Otto and W. Sohler, "Modification of the total reflection modes in a dielectric film by one metal boundary," *Opt. Commun.* **3**(4), 254–258 (1971).